AGU PUBLICATIONS

Geophysical Research Letters

RESEARCH LETTER
10.1002/2016GL068576

Key Points:
- Ocean alkalinization simulations based on the RCPs performed with the emissions-driven Max Planck Institute Earth System model
- Atmospheric CO_2 reduction via alkalinization may rise pH and omega to greater than modern ocean levels
- Regionally inhomogeneous pH and omega response due to the particular biophysicochemical ocean regimes

Supporting Information:
- Supporting Information S1

Correspondence to:
M. F. González,
miriam.ferrer-gonzalez@mpimet.mpg.de

Citation:
González, M. F., and T. Ilyina (2016), Impacts of artificial ocean alkalinization on the carbon cycle and climate in Earth system simulations, *Geophys. Res. Lett.*, *43*, 6493–6502, doi:10.1002/2016GL068576.

Received 21 MAR 2016
Accepted 23 MAY 2016
Accepted article online 28 MAY 2016
Published online 21 JUN 2016

The copyright line for this article was changed on 22 JUL 2016 after original online publication.

Impacts of artificial ocean alkalinization on the carbon cycle and climate in Earth system simulations

Miriam Ferrer González[1,2] and Tatiana Ilyina[1]

[1] Max Planck Institute for Meteorology, Hamburg, Germany, [2] International Max Planck Research School on Earth System Modeling, Hamburg, Germany

Abstract Using the state-of-the-art emissions-driven Max Planck Institute Earth system model, we explore the impacts of artificial ocean alkalinization (AOA) with a scenario based on the Representative Concentration Pathway (RCP) framework. Addition of 114 Pmol of alkalinity to the surface ocean stabilizes atmospheric CO_2 concentration to RCP4.5 levels under RCP8.5 emissions. This scenario removes 940 GtC from the atmosphere and mitigates 1.5 K of global warming within this century. The climate adjusts to the lower CO_2 concentration preventing the loss of sea ice and high sea level rise. Seawater pH and the carbonate saturation state (Ω) rise substantially above levels of the current decade. Pronounced differences in regional sensitivities to AOA are projected, with the Arctic Ocean and tropical oceans emerging as hot spots for biogeochemical changes induced by AOA. Thus, the CO_2 mitigation potential of AOA comes at a price of an unprecedented ocean biogeochemistry perturbation with unknown ecological consequences.

1. Introduction

Geoengineering techniques have been suggested to tackle climate change and ocean acidification; however, knowledge about their effectiveness and side effects remains sparse [e.g., *The Royal Society*, 2009; *National Research Council*, 2015]. Artificial ocean alkalinization (AOA) is one of the ocean-based carbon dioxide removal (CDR) methods that aims at enhancing the natural and slow (timescales of 10k-100k years) process of weathering by which CO_2 is taken out of the atmosphere via chemical sequestration [e.g., *Kheshgi*, 1995; *Hartmann et al.*, 2013]. Total alkalinity (TA) describes the charge balance of weak ions in seawater [*Wolf-Gladrow et al.*, 2007], and the method of ocean alkalinization involves the release of processed alkaline minerals (e.g., olivine, calcium carbonate), or their dissociation products (e.g., quicklime, calcium hydroxide) at the ocean-atmosphere interface. By increasing surface TA, CO_2 uptake and storage is enhanced and the buffering capacity of seawater is modified such that seawater pH increases. The amount of added alkalinity varies depending upon the used chemical substance.

Previous modeling studies have addressed some aspects of AOA. For instance, *Ilyina et al.* [2013a] based on an ocean stand-alone model configuration, showed that addition of large amounts of alkalinity might elevate Ω to values at which inorganic fallout of $CaCO_3$ starts, thereby reaching a natural biogeochemical threshold of AOA. A study with an Earth system model of intermediate complexity [*Keller et al.*, 2014], constrained by present-day transport capacity and thus adding small amounts of alkalinity, suggested a low potential of AOA to mitigate atmospheric CO_2 rise. *Köhler et al.* [2013], studying olivine-based alkalinity enhancement projected changes in the marine biology and biological carbon pumps due to the silicic acid enrichment associated with AOA using olivine. The greatest impact on marine biology of AOA via olivine dissolution, however, was shown to be due to the concomitant iron enrichment [*Hauck et al.*, 2016].

While the effects of AOA on marine biota are not yet fully understood, a laboratory study reveals that addition of alkalinity could disrupt the acid base balance of marine organisms such as littoral crabs [*Cripps et al.*, 2013]. Besides, the addition of alkaline substances releases conjointly toxic heavy metals (e.g., cadmium, nickel, chromium) leading to further perturbations that would likely impact ocean biogeochemical cycling and marine ecosystem services [e.g., *Hartmann et al.*, 2013; *Hauck et al.*, 2016].

We explore an idealized alkalinity enhancement scenario focusing on the current century based on the representative concentration pathways (RCP) scenarios of climate change. We use the Max Planck Institute

Earth System Model (MPI-ESM) in the configuration of the fifth phase Coupled Model Intercomparison Project (CMIP5) [*Giorgetta et al.*, 2013] forced by fossil fuel CO_2 emissions. By testing the high CO_2 emission scenario RCP8.5, we address the question whether in a high CO_2 world following the RCP8.5 scenario, it is possible to stabilize atmospheric CO_2 to RCP4.5 levels by AOA alone. If so, how much does the buffering capacity of the ocean need to be enhanced? What will be the consequences of such a large-scale AOA scenario in the Earth system? We also address the response of the different ocean basins to AOA, revealing the different regional sensitivities to increasing seawater TA. Despite the inherent limitations of AOA (e.g., finite shipping capacity and high-energy demands), we solely focus on the response of the Earth system to this geoengineering method.

2. Methodology

2.1. Model Description

In the ocean biogeochemical model HAMOCC (HAMburg Ocean Carbon Cycle model), which is part of MPI-ESM, seawater TA varies due to $CaCO_3$ formation and dissolution, CO_2 fixation and respiration by biota, changes in freshwater and weathering fluxes as well as seawater-sediment interaction. Natural weathering fluxes of $CaCO_3$ and silicate are prescribed so that they compensate the losses of these materials to the sediments [*Ilyina et al.*, 2013b]. The globally uniform input of $CaCO_3$ does not vary over time and increases the TA content by 56.84 TmolC/yr in all the scenarios described in this study. Dissolved inorganic carbon (DIC) is altered not only due to these natural processes that vary TA but also due to atmosphere-ocean gas exchange. Variations in the DIC to TA ratio determine hydrogen ion concentrations and therefore seawater pH. HAMOCC is embedded into the free-surface ocean circulation model (MPIOM) including a sea ice component; both modules have a nominal resolution of 1.5° and 40 unevenly spaced vertical levels [*Jungclaus et al.*, 2013]. Terrestrial biogeochemistry and land-atmosphere interaction are simulated with the land vegetation model JSBACH [*Reick et al.*, 2013], which is directly coupled to the atmospheric general circulation model (ECHAM6) [*Stevens et al.*, 2013] and runs on the same horizontal grid (1.9° horizontal grid resolution and 47 pressure levels). This is the low-resolution version of the emissions-driven MPI-ESM as used in CMIP5 [*Giorgetta et al.*, 2013].

2.2. Alkalinization Scenario

Alkalinity enhancement is designed to stabilize the increasing atmospheric CO_2 concentration of the RCP8.5 to RCP4.5 levels (Figure 1d). The cumulative carbon emissions of the RCP8.5 scenario (~1850 GtC) are higher than those of the RCP4.5 by around 940 GtC by the year 2100 (Figure S1a). The RCPs reference simulations are calculated with the MPI-ESM and their description can be found in *van Vuuren et al.* [2011]. RCP4.5 takes into account mitigation efforts and therefore different (than RCP8.5) land management, air pollutants, and greenhouse gases emissions are assumed. Land use transitions and emissions of air pollutants and greenhouse gases (such as CO_4, N_2O, and CFCs) in the alkalinization scenario are given by the RCP8.5 scenario. Alkalinity is added every time step increasingly over time and spatially homogeneous (same amount per unit area) into the first ocean model level including oceanic areas covered by sea ice (i.e., first 12 m modified by the surface elevation). DIC, nutrients or trace metals are not added during the alkalinization scenarios. The simulation starts in 2006 and AOA begins when atmospheric CO_2 differs from the one of the RCP4.5 scenario by around 1% (year 2018). AOA lasts until 2100 when also the simulation period ends. Model internal variability is addressed with an ensemble of three members. The forcing in each run is identical, but they were initialized from the end of different ensemble members of historical CMIP5 experiments [*Giorgetta et al.*, 2013].

3. Fate of Added Alkalinity

In order to maintain atmospheric CO_2 at RCP4.5 levels under the high-emission scenario RCP8.5, $\approx 114 \cdot 10^{15}$ mol (Pmol) of added alkalinity would be needed until the year 2100 in total (Figure 1a). This implies an increase in the globally averaged surface TA concentration of around 30%. In order to produce 114 Pmol of TA, about $4.01 \cdot 10^{12}$ metric tons (Tt) of olivine would be needed, which would require an increase of 3 orders of magnitude in the total olivine production until 2100. The total production of lime until 2100 would need to be enhanced by 2 orders of magnitude to supply around 4.22 Tt of lime which are required to produce 114 Pmol of TA (details of these estimations can be found in the supporting information).

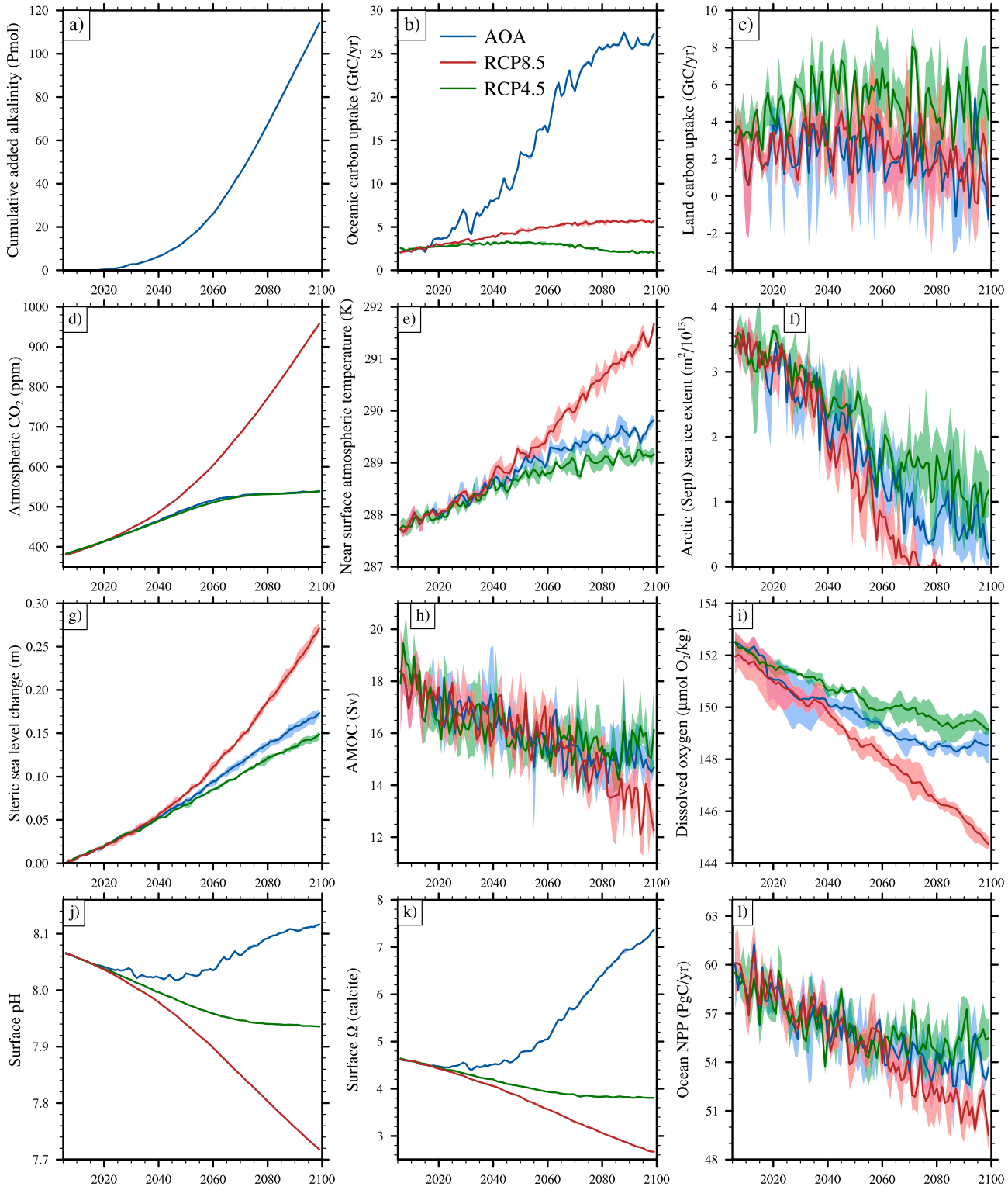

Figure 1. Temporal evolutions of various Earth system variables in different scenarios. Solid lines depict 3 year running means under the scenarios RCP8.5 (red), AOA (blue), and RCP4.5 (green). (a) Cumulative added alkalinity (Pmol), (b) total ocean carbon uptake per year (Gt/yr), (c) total terrestrial carbon uptake per year (Gt/yr), (d) global annual mean of atmospheric CO_2 (ppm), (e) global annual mean of near-surface atmospheric temperature (K), (f) monthly mean (September) of Arctic sea ice extent (m^2), (g) global annual mean of steric sea level rise (m), (h) Atlantic meridional overturning circulation zonally averaged at 26°N (Sv; sverdrup (10^6 m^3/s)), (i) global annual mean of O_2 concentration vertically averaged over 200–600 m (µmol O_2/kg), (j) global annual mean of surface seawater pH, (k) global annual mean of surface Ω with respect to calcite, (l) global annual mean of ocean net primary production (NPP) vertically integrated (PgC/yr). Colored area is model internal variability including three ensemble members.

The amount of needed alkalinity increases over time due to the growing atmospheric CO_2 concentrations of the RCP8.5 scenario (up to 950 ppm in 2100 (Figure 1d)). The fate of added alkalinity is different in each ocean basin due to its dissimilar current dynamics (Figure S3). Surface TA in the Atlantic, Pacific, and the Indian Ocean basins, increments by ~0.05% (relative to their present-day value) in 2045. Then, surface TA further increases over time so that at the end of this century in both the south Atlantic and the entire Pacific, present-day TA is exceeded by ~35% (i.e., from an initial value of ~2.300 μmol/kg to ~3.100 μmol/kg in a time-lapse of 55 years). Even higher values are reached in the north Atlantic and Indian Oceans (up to 50% higher than present-day levels). Alkalinity is only added in the first 12 m of the ocean (± surface elevation), and then it is mixed with deeper water masses through the processes of advection and diffusion. This vertical mixing leads to TA changes in these basins reaching water masses within the first 1000 m of the water column during the last decades of this century. The Arctic and Southern Oceans present a different temporal and spatial evolution compared to other ocean basins and between each other. This is due to the volume of water involved in the dissolution of the added alkalinity which is, comparing all the basins, much lower in the Arctic and much higher in the Southern Ocean, leading to a different increment of TA per unit volume in these two basins.

4. Impact on Carbon Uptake and Storage

In the modern ocean, tropical and subtropical regions act as sources of carbon to the atmosphere [*Takahashi et al.*, 2009]. The MPI-ESM projects some of these regions to change from source to sink of carbon at the end of this century under the RCP8.5 high emission scenario (Figure S2). In the alkalinization experiment, all regions of the ocean absorb atmospheric carbon due to the changes in the buffering capacity. The equator presents the lowest carbon uptake (~20 gC/m^2) while areas within latitudes from 30° to 80° show the highest values (~100 gC/m^2). The globally integrated uptake of carbon by the ocean responds linearly to the addition of TA (Figure S1b), with much lower variability compared to the globally integrated carbon uptake by land (Figure S1c).

The enhanced oceanic CO_2 uptake (Figure 1b) in the AOA scenario greatly increases the marine DIC pool (Figure 2). Compared to the RCP8.5, the vertically integrated increase in DIC content by 2100 is up to 1 order of magnitude higher in some regions, as, for instance, the high latitudes of the North Atlantic Ocean (i.e., increasing from around 2–5 kgC/m^2 in RCP8.5 and up to 10–15 kgC/m^2 in the AOA scenario). Because of the great volume of seawater involved in the transport of carbon in the Southern Ocean, the DIC increment per unit volume is much smaller compared to the other basins (Figure S4). Changes in carbon uptake and storage over land in the AOA scenario are similar to those associated with the RCP8.5 scenario (Figures 1c and 2). However, carbon storage over land is slightly lower in the AOA scenario compared to the RCP8.5 due to the decrease in atmospheric CO_2 concentration that lowers the CO_2 fertilization effect on the terrestrial biosphere. Variations in land carbon uptake and storage in our AOA scenario relative to RCP4.5 are due to anthropogenic land use, CO_2 fertilization [*Schneck et al.*, 2013] and regional changes in temperature and precipitation [*Giorgetta et al.*, 2013; *Reick et al.*, 2013].

5. Effects on the Climate System

The alkalinization scenario leads to a large oceanic carbon uptake enhancement (up to 27 GtC/yr at the end of this century) (Figure 1b) and therefore much lower atmospheric CO_2 concentrations and surface atmospheric temperatures (Figures 1d and 1e). Compared to the reference scenario RCP8.5, the AOA experiment leads to a reduction in the annual global mean of air surface temperature of around 1.5 K, following more closely the RCP4.5 scenario. The slightly higher temperature (0.5 K) of AOA compared to RCP4.5 is because AOA only reduces atmospheric CO_2 so that the other greenhouse gases (GHGs) remain unmitigated. Not only GHGs emissions differ between RCP8.5 and RCP4.5, land use and pollutant emissions are also specifically defined for each scenario. Because of that, differences in the state of the climate between the targeted (solely in terms of atmospheric CO_2 levels) RCP4.5 and the strongly mitigated RCP8.5 by means of the AOA scenario are expectable.

Boreal summer sea ice extent is projected to shrink as global temperature rises during the 21st century [*Intergovernmental Panel on Climate Change (IPCC)*, 2013; *Notz et al.*, 2013]. While the summer sea ice is projected to disappear under the RCP8.5 scenario around the year 2070 (Figure 1f), this does not occur under the AOA scenario, even so a reduction to ~15% of its current value (i.e., to $\approx 5 \cdot 10^{12}$ m^2) is obtained because of

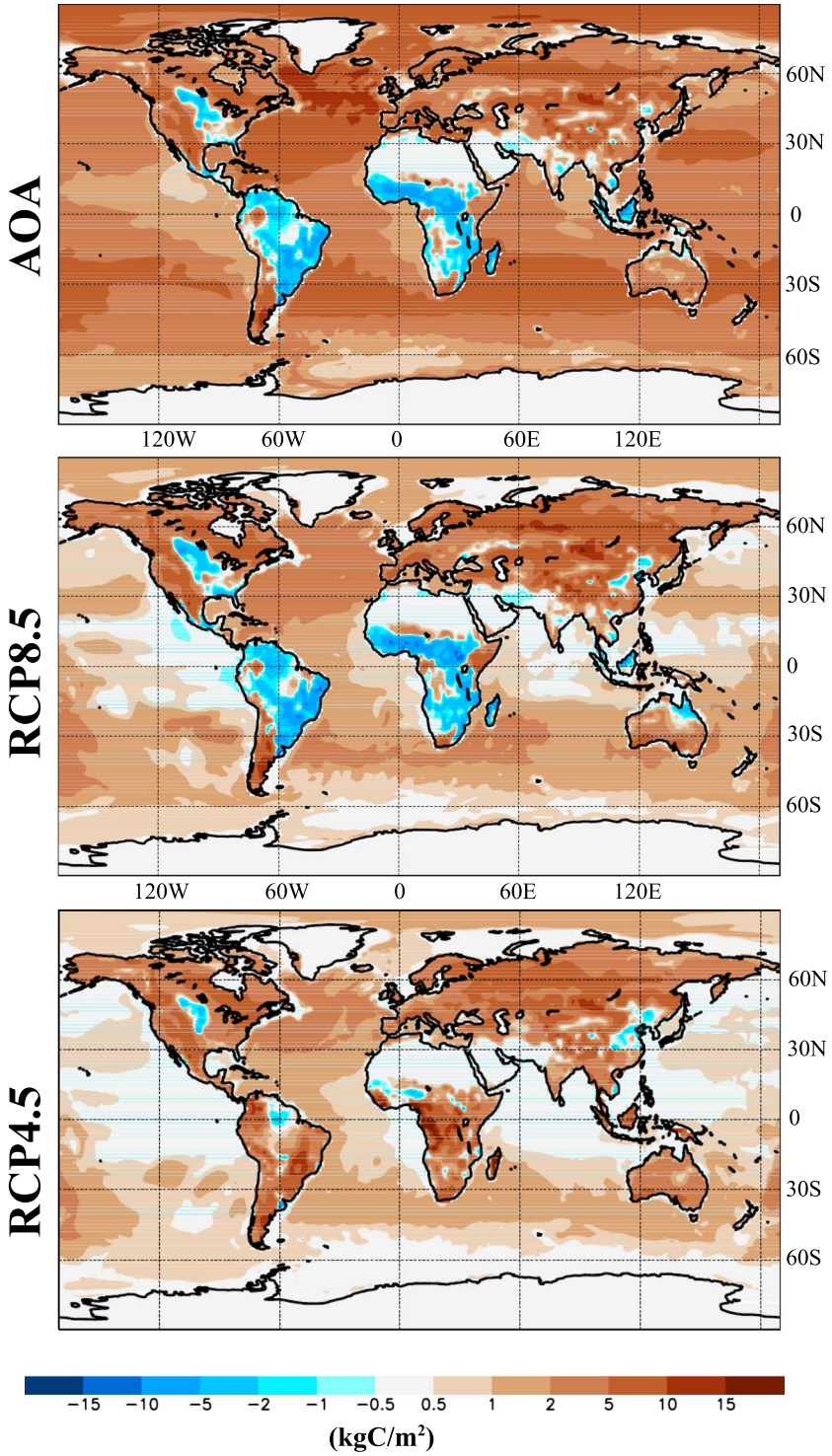

Figure 2. Changes in the terrestrial and oceanic carbon budgets: difference between the annual mean carbon reservoirs (vertically integrated) of the year 2100 and the year 2006 in the scenarios (top) AOA, (middle) RCP8.5, and (bottom) RCP4.5 (bottom). Note the nonlinear color bar.

the higher temperatures relative to the current climate state. Such slightly higher temperatures are also the reason why this geoengineering scenario only reduces ~75% of the projected steric (due to thermal expansion) sea level rise in the RCP8.5, differing from the targeted RCP4.5 by ~0.03 m (Figure 1g). The Atlantic Meridional Overturning Circulation (AMOC) has been projected to weaken under the RCP8.5 scenario

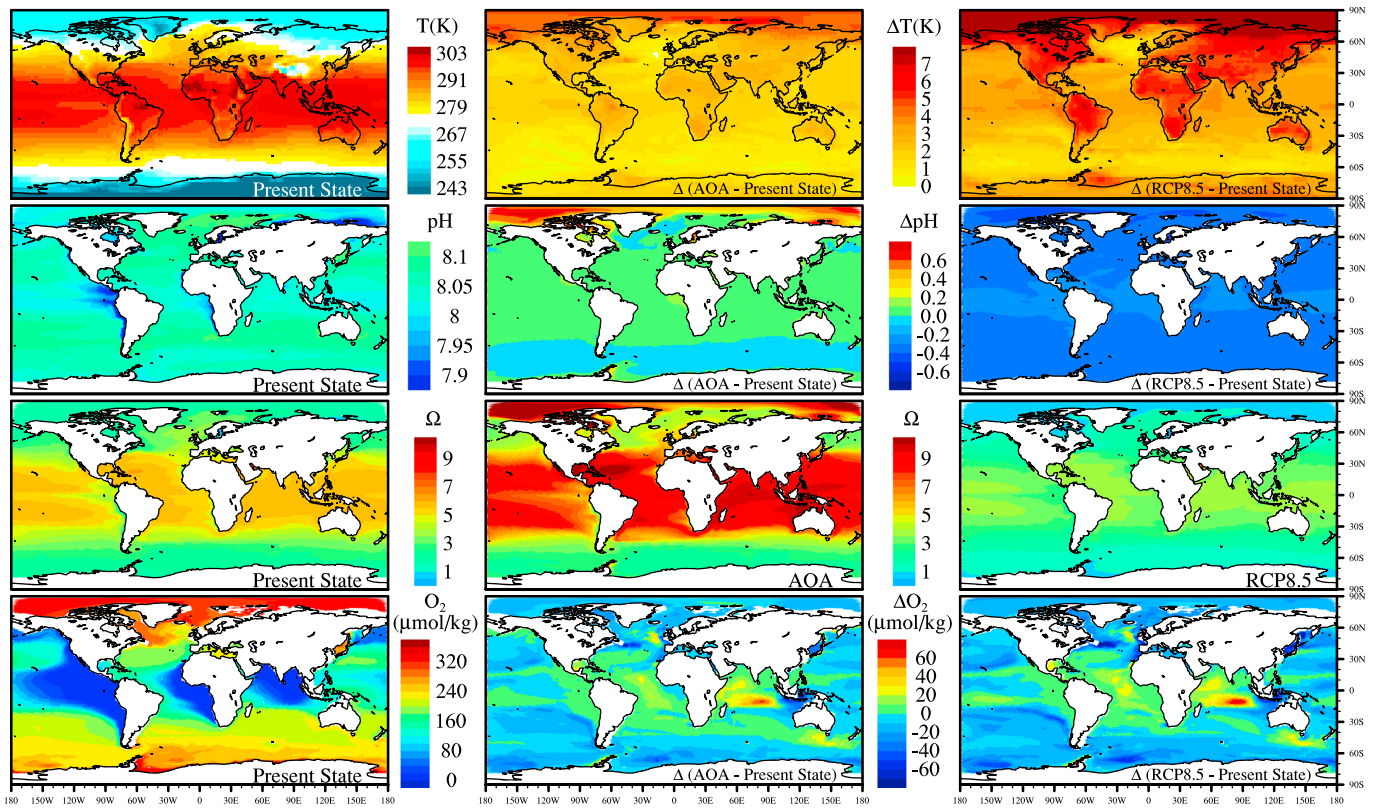

Figure 3. Annual means (averaged over 10 years period) and anomalies of near-surface atmospheric temperature (first row), surface seawater pH (second row), surface seawater Ω (third row) with respect to calcite and O_2 concentration vertically averaged over intermediate waters (200–600 m water depth, fourth row). (left column) Present-day state (2006–2015); Differences between the AOA (2090-2099, middle column) and the RCP8.5 (2090–2099, right column) scenarios and present-day state except for the 3rd row where only absolute values of Ω are depicted. Color-bars for the maps in the left column are to their right side. Maps in the middle and right columns share the color bars located between them.

[*IPCC*, 2013]. This weakening is reduced under the AOA scenario leading to a similar value than the one projected under the RCP4.5 scenario (Figure 1h).

The above mentioned set of variables present different ranges of internal model variability. For instance, the internal model variability of oceanic carbon uptake and atmospheric CO_2 levels is small and is driven by the trajectory prescribed by the emissions scenarios. In contrast, variability associated with parameters such as the Arctic summer sea ice, terrestrial carbon uptake, and the AMOC is much larger (up to 1 order of magnitude lower than the values of these parameters). In spite of the large internal model variability in some of the variables, the AOA signal is clear and trends are consistent among different ensemble members.

Regarding regional differences in near-surface atmospheric temperatures (Figure 3), the higher effect is found in the Arctic due to the Arctic amplification and over the continents due to the different heat capacity of land and ocean surfaces. Compared with the unmitigated RCP8.5, the large-scale AOA scenario prevents ~2.8 K of warming over the Arctic and the subpolar regions of the North hemisphere.

6. Effects on Ocean Biogeochemistry

The AOA scenario strongly mitigates ocean acidification over the whole period of integration, albeit leading to much higher global surface ocean pH and Ω (calcite) values than those of the RCP4.5 scenario (Figures 1j and 1k). In the last decades of this century, higher than present-day values of surface ocean pH are reached. Regarding Ω, higher than modern ocean levels are achieved from 2050 until the end of the simulated period.

Considering regional surface seawater values (Figure 3), under the RCP8.5 scenario pH and Ω decline so that, for instance, most of the Arctic Ocean becomes undersaturated by the end of the century in our model. AOA mitigates ocean acidification effects, but modern ocean pH and Ω values are strongly exceeded in several regions, which is an unintended consequence of this method that may induce negative effects on marine

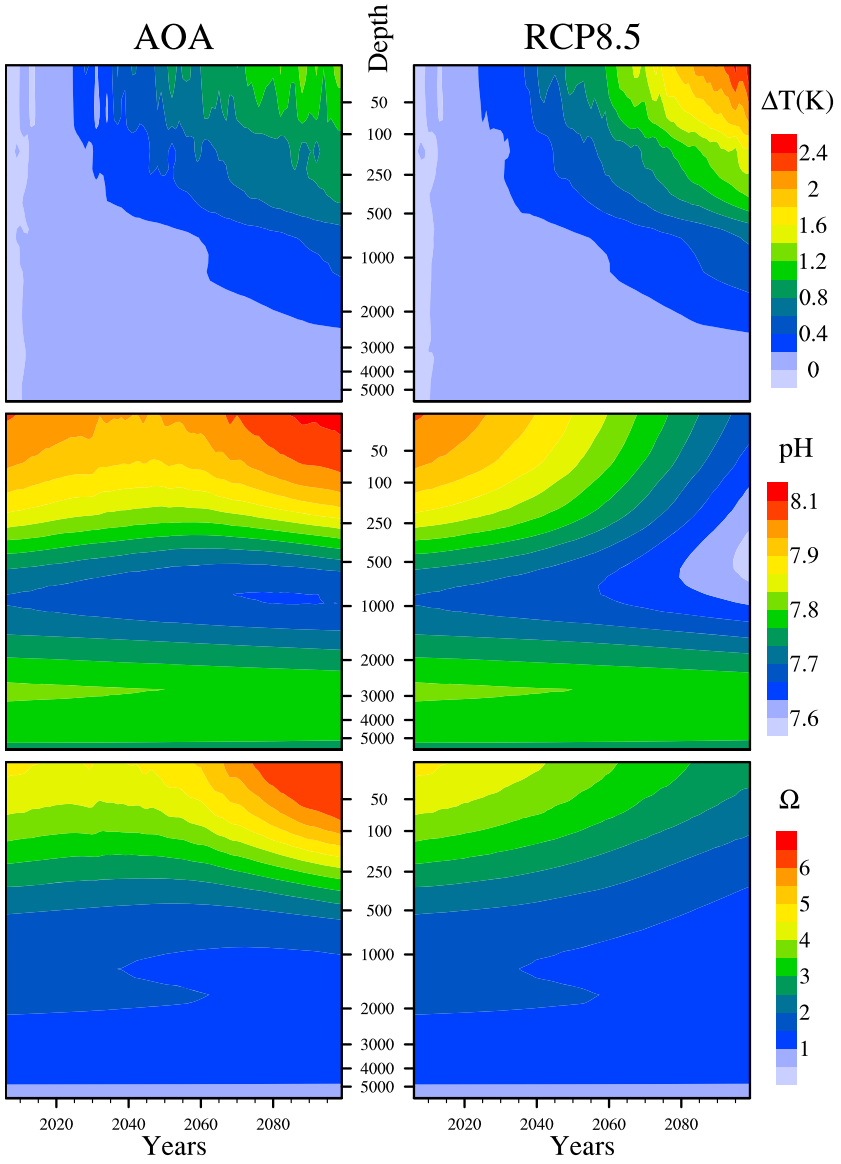

Figure 4. Temporal evolution of the vertical profiles (globally averaged annual means) of seawater potential temperature anomaly with respect to present-day ocean state (2006–2015), absolute values of seawater pH and Ω with respect to calcite under the experiments (left column) AOA and (right column) RCP8.5. Note the nonlinear vertical axis in which resolution decreases with depth.

biota [e.g., *Cripps et al.*, 2013; *Haigh et al.*, 2015]. As a result of our idealized implementation scheme, in large regions of the Arctic Ocean, surface seawater pH greatly exceeds current levels. Besides, much higher levels of supersaturation are also reached in the Arctic surface seawater regionally (5 times larger than modern ocean levels) and in most of the tropical and subtropical oceans (doubling present-day values). Hence, a large-scale AOA scenario, along with perturbations in the biogeochemical cycles due to warming [e.g., *Vancoppenolle et al.*, 2013; *Steiner et al.*, 2014], is likely to cause strong unintended side effects in these ocean basins. Still, values higher than 20 (best current estimate but not well constrained), when inorganic sinking of $CaCO_3$ is estimated to be triggered [*Morse and He*, 1993], are not obtained in the open ocean.

Within this century, the MPI-ESM under the RCP8.5 scenario projects the most pronounced decrease in global mean pH and Ω within approximately the upper 500 m of the water column (Figures 4, S7, and S9). This is consistent with CMIP5 models [e.g., *Bopp et al.*, 2013; *Gehlen et al.*, 2014]. In tropical oceans where warm-water corals grow, Ω values largely drop. These changes in seawater pH and Ω do not occur under the AOA scenario (Figures 4, S6, and S8). Between ≈250 and 1000 m depth, pH and Ω are restored to levels of the modern ocean

during the last decades of this century. However, as a side effect in most of the ocean basins, modern levels are exceeded in shallower than 250 m depth. At deeper levels than 1000 m under the AOA scenario, the propagation of ocean acidification continues. Over time scales of several centuries, the ocean acidification signal would reach the bottom ocean and trigger reaction with carbonate sediments [*Ilyina and Zeebe*, 2012]. Thus, in the course of the 21st century, large-scale AOA can only partially prevent the projected deep ocean acidification [*Gehlen et al.*, 2014]. These are general features present in most of the ocean basins. Still, the response of each basin under the strong AOA mitigation shows differences; indicating different seawater pH and Ω sensitivities owing to their particular physical and biogeochemical states. In the Southern Ocean, seawater pH and Ω remain similar to present-day values over the whole period of integration under the AOA scenario because of its fairly constant DIC to TA ratio over time (Figure S5). The Indian, Atlantic, Pacific and Arctic Oceans show different sensitivities to the homogeneous alkalinization, with the Indian basin reaching the highest Ω levels in the upper 250 m. The response to AOA of the carbonate system in this study is consistent with results of previous studies where different model setups have been used under different AOA scenarios [e.g., *Köhler et al.*, 2013; *Ilyina et al.*, 2013a; *Keller et al.*, 2014]. The obtained high values of pH and Ω are driven by the large-scale alkalinization assumed with large amounts of alkalinity being added in our experimental design. Compared to the current ocean state, the higher Ω values at deeper ocean layers under the AOA scenario for all the ocean basins during the last decades of this century (Figure S8), imply a deepening of the calcite saturation horizon ($\Omega = 1$) and lower $CaCO_3$ dissolution rates at these depths. The opposite effect occurs under the RCP8.5 scenario. Ocean acidification lowers Ω within the water column (Figure S9), increasing the $CaCO_3$ dissolution rates at these depths and shallowing the calcite saturation horizon.

Changes in the ocean thermal state indirectly driven by AOA (via atmospheric CO_2 reduction) penetrate until similar depths as the pH and Ω signals (Figure 4). Besides, these changes in the thermal state show a much more homogeneous vertical profile, not only compared to the above discussed biogeochemical variables but also compared to the thermal state anomaly under the RCP8.5 scenario. This is due to the lower rate of warming over time and the concomitant lower thermal stratification in the AOA scenario relative to the RCP8.5.

Ocean biogeochemistry is not only directly affected by AOA, it is also indirectly altered through changes in the climate state brought about by alkalinity enhancement. For instance, marine net primary production is projected to decrease over time under the high emission scenario RCP8.5 (Figure 1l). This is due to higher nutrient limitation driven by an enhancement in ocean thermal stratification [*Bopp et al.*, 2013]. The mitigated ocean warming under the AOA scenario decreases such an enhanced stratification. Besides, in case of using olivine, net primary production might be further boosted in the AOA scenario due to the addition of iron and silicic acid [e.g., *Hauck et al.*, 2016; *Köhler et al.*, 2013]. The projected decline in oxygen at middepths (within the upper 200–600 m) is also indirectly mitigated by the AOA scenario. Temporal evolution of oxygen at middepths (global annual means) paralelly follows the RCP4.5 projection hampering the steep decline under the RCP8.5 scenario (Figure 1i). Regionally, changes in oxygen indirectly driven by AOA follow the same spatial patterns projected in the RCP8.5, however the magnitude of change is reduced (Figure 3). Internal model variability is much lower in pH and Ω values and higher for ocean net primary production and oxygen concentrations. This is confirmed in previous modeling studies, suggesting high (but likely underestimated in ESMs) internal variability of oxygen concentration variations [e.g., *Andrews et al.*, 2013]. However, temporal trends are consistent and it is clear that the state of the system is close to one of the RCP4.5 scenarios.

7. Summary and Conclusions

We focus on the consequences of a large-scale AOA scenario in the Earth system in which atmospheric CO_2 concentrations of the RCP8.5 scenario are reduced to RCP4.5 levels until the year 2100 after addition of ca. 114 Pmol of alkalinity. This large amount of added alkalinity determines the response of the Earth system. The entire ocean turns into a carbon sink removing of 940 GtC from the atmosphere. The global warming of the RCP8.5 world is mitigated by about 1.5 K at the end of this century. The 0.5 K higher global surface atmospheric temperature of the AOA scenario compared to the targeted RCP4.5 is due to the radiative forcing effect of non-CO_2 GHGs. Arctic sea ice extent and steric sea level rise adjust to the slightly warmer (than RCP4.5) climate state with the extreme sea level rise and ice loss being prevented. Biogeochemical parameters such as oxygen and net primary production behave in accordance to the changes in the climate system, albeit indicating large internal variability.

The enhanced ocean carbon uptake and storage nearly doubles the marine DIC content increase projected under the RCP8.5 scenario by 2100. This invasion of CO_2 into the ocean would lead to stronger acidification than the one projected under the RCP8.5 and RCP4.5 scenarios. Yet, the alkalinization fully compensates the decreasing seawater pH with the side effect of surface pH and Ω values exceeding levels of the modern ocean. Given the length of our simulation, AOA only partially addresses effects of climate change and ocean acidification in the deep ocean.

Our AOA scenario reveals the different regional sensitivities to increasing seawater TA. Alkalinity addition is spatially homogeneous. Still, pronounced regional differences arise on the pH and Ω response to AOA due to the varying physical regimes and biogeochemical states of the different ocean basins. In our alkalinization scenario, the Arctic Ocean is a hot spot for unintended changes brought about by a large-scale AOA. This is because a dissimilar rise of DIC and TA under the AOA scenario, increases surface seawater pH (up to 0.6 higher units) and Ω (fivefold increase) to greater than modern ocean levels. In the tropical oceans, surface Ω doubles present-day values due to synergies between growing seawater temperatures and increasing carbonate concentrations. Thus, the strong CO_2 removal potential of AOA implicates an unprecedented ocean biogeochemistry perturbation. The consequences of these regional perturbations in the seawater chemical environment are completely unknown, but they may be negative, not only due to the magnitude of the changes but also owing to their pace.

Acknowledgments

This research was supported by the German Science Foundation (DFG) within the Priority Program Climate Engineering: Risks, Challenges, Opportunities (SPP 1689). Computational resources were made available by the German Climate Computing Center (DKRZ) through support from the German Federal Ministry of Education and Research (BMBF). We thank Irene Stemmler for her help and useful comments on this manuscript. Primary data and scripts needed to reproduce this analysis are archived by the Max Planck Institute for Meteorology and will be available by contacting publications@mpimet.mpg.de.

References

Andrews, O. D., N. L. Bindoff, P. R. Halloran, T. Ilyina, and C. Le Quéré (2013), Detecting an external influence on recent changes in oceanic oxygen using an optimal fingerprinting method, *Biogeosciences*, *10*(3), 1799–1813, doi:10.5194/bg-10-1799-2013.

Bopp, L., et al. (2013), Multiple stressors of ocean ecosystems in the 21st century: Projections with CMIP5 models, *Biogeosci. Discuss.*, *10*(2), 3627–3676, doi:10.5194/bgd-10-3627-2013.

Cripps, G., S. Widdicombe, J. I. Spicer, and H. S. Findlay (2013), Biological impacts of enhanced alkalinity in Carcinus maenas, *Mar. Pollut. Bull.*, *71*(1–2), 190–198, doi:10.1594/PANGAEA.829880.

Gehlen, M., et al. (2014), Projected pH reductions by 2100 might put deep North Atlantic biodiversity at risk, *Biogeosciences*, *11*(23), 6955–6967, doi:10.5194/bg-11-6955-2014.

Giorgetta, M. A., et al. (2013), Climate and carbon cycle changes from 1850 to 2100 in MPI-ESM simulations for the coupled model intercomparison project phase 5, *J. Adv. Model. Earth Syst.*, *5*, 572–597, doi:10.1002/jame.20038.

Haigh, R., D. Ianson, C. A. Holt, H. E. Neate, and A. M. Edwards (2015), Effects of ocean acidification on temperate coastal marine ecosystems and fisheries in the Northeast Pacific, *PLoS ONE*, *10*(2), e0117533, doi:10.1371/journal.pone.0117533.

Hartmann, J., A. J. West, P. Renforth, P. Köhler, C. L. De La Rocha, D. A. Wolf-Gladrow, H. H. Dürr, and J. Scheffran (2013), Enhanced chemical weathering as a geoengineering strategy to reduce atmospheric carbon dioxide, supply nutrients, and mitigate ocean acidification, *Rev. Geophys.*, *51*, 113–149, doi:10.1002/rog.20004.

Hauck, J., P. Köhler, D. Wolf-Gladrow, and C. Völker (2016), Iron fertilisation and century-scale effects of open ocean dissolution of olivine in a simulated CO_2 removal experiment, *Environ. Res. Lett.*, *11*(2), 024007.

Ilyina, T., and R. E. Zeebe (2012), Detection and projection of carbonate dissolution in the water column and deep-sea sediments due to ocean acidification, *Geophys. Res. Lett.*, *39*, L06606, doi:10.1029/2012GL051272.

Ilyina, T., D. Wolf-Gladrow, G. Munhoven, and C. Heinze (2013a), Assessing the potential of calcium-based artificial ocean alkalinization to mitigate rising atmospheric CO_2 and ocean acidification, *Geophys. Res. Lett.*, *40*, 5909–5914, doi:10.1002/2013GL057981.

Ilyina, T., K. D. Six, J. Segschneider, E. Maier-Reimer, H. Li, and I. Núñez Riboni (2013b), Global ocean biogeochemistry model HAMOCC: Model architecture and performance as component of the MPI-Earth system model in different CMIP5 experimental realizations, *J. Adv. Model. Earth Syst.*, *5*, 287–315, doi:10.1029/2012MS000178.

Intergovernmental Panel on Climate Change (IPCC) (2013), Climate Change 2013: The Physical Science Basis, *Contribution of Working Group I to the Fifth Assessment Report of the Intergovernmental Panel on Climate Change*, Cambridge Univ. Press, Cambridge, U. K., and New York, doi:10.1017/CBO9781107415324.

Jungclaus, J. H., N. Fischer, H. Haak, K. Lohmann, J. Marotzke, D. Matei, U. Mikolajewicz, D. Notz, and J. S. von Storch (2013), Characteristics of the ocean simulations in the Max Planck Institute Ocean Model (MPIOM) the ocean component of the MPI-Earth system model, *J. Adv. Model. Earth Syst.*, *5*, 422–446, doi:10.1002/jame.20023.

Keller, D. P., E. Y. Feng, and A. Oschlies (2014), Potential climate engineering effectiveness and side effects during a high carbon dioxide-emission scenario, *Nat. Commun.*, *5*, 3304, doi:10.1038/ncomms4304.

Kheshgi, H. S. (1995), Sequestering atmospheric carbon dioxide by increasing ocean alkalinity, *Energy*, *20*(9), 915–922.

Köhler, P., J. F. Abrams, C. Völker, J. Hauck, and D. Wolf-Gladrow (2013), Geoengineering impact of open ocean dissolution of olivine on atmospheric CO_2, surface ocean pH and marine biology, *Environ. Res. Lett.*, *8*(1), 014009, doi:10.1088/1748-9326/8/1/014009.

Morse, J. W., and S. He (1993), Influences of T, S and P_{CO_2} on the pseudo-homogeneous precipitation of $CaCO_3$ from seawater: Implications for whiting formation, *Mar. Chem.*, *41*(4), 291–297, doi:10.1016/0304-4203(93)90261-L.

National Research Council (2015), *Climate Intervention: Carbon Dioxide Removal and Reliable Sequestration*, The National Academies Press, Washington, D. C.

Notz, D., F. A. Haumann, H. Haak, J. H. Jungclaus, and J. Marotzke (2013), Arctic sea-ice evolution as modeled by Max Planck Institute for Meteorology's Earth system model, *J. Adv. Model. Earth Syst.*, *5*, 173–194, doi:10.1002/jame.20016.

Reick, C. H., T. Raddatz, V. Brovkin, and V. Gayler (2013), Representation of natural and anthropogenic land cover change in MPI-ESM, *J. Adv. Model. Earth Syst.*, *5*, 459–482, doi:10.1002/jame.20022.

Schneck, R., C. H. Reick, and T. Raddatz (2013), Land contribution to natural CO_2 variability on time scales of centuries, *J. Adv. Model. Earth Syst.*, *5*, 354–365, doi:10.1002/jame.20029.

Steiner, N. S., J. R. Christian, K. D. Six, A. Yamamoto, and M. Yamamoto-Kawai (2014), Future ocean acidification in the Canada Basin and surrounding Arctic Ocean from CMIP5 Earth system models, *J. Geophys. Res. Oceans*, *119*, 332–347, doi:10.1002/2013JC009069.

Stevens, B., et al. (2013), Atmospheric component of the MPI-M Earth system model: ECHAM6, *J. Adv. Model. Earth Syst.*, *5*, 146–172, doi:10.1002/jame.20015.

Takahashi, T., et al. (2009), Climatological mean and decadal change in surface ocean P_{CO_2}, and net sea-air CO_2 flux over the global oceans, *Deep Sea Res., Part II*, *56*(8–10), 554–577, doi:10.1016/j.dsr2.2008.12.009.

The Royal Society (2009), *Geoengineering the Climate: Science, Governance and Uncertainty*, London.

van Vuuren, D., et al. (2011), The representative concentration pathways: An overview, *Clim. Change*, *109*(1–2), 5–31, doi:10.1007/s10584-011-0148-z.

Vancoppenolle, M., L. Bopp, G. Madec, J. Dunne, T. Ilyina, P. R. Halloran, and N. Steiner (2013), Future Arctic Ocean primary productivity from CMIP5 simulations: Uncertain outcome, but consistent mechanisms, *Global Biogeochem. Cycles*, *27*, 605–619, doi:10.1002/gbc.20055.

Wolf-Gladrow, D. A., R. E. Zeebe, C. Klaas, A. Körtzinger, and A. G. Dickson (2007), Total alkalinity: The explicit conservative expression and its application to biogeochemical processes, *Mar. Chem.*, *106*(1–2), 287–300.